Ion-ion and electron-ion correlations in liquid metallic sodium calculated from the nucleus-electron model

1992 J. Phys.: Condens. Matter 4 3679

(http://iopscience.iop.org/0953-8984/4/14/003)

J. Phys.: Condens. Matter 4 (1992) 3679–3694. Printed in the UK

Ion–ion and electron–ion correlations in liquid metallic sodium calculated from the nucleus–electron model

M Ishitobi† and J Chihara‡

† Department of Physics, Faculty of Science, Kanazawa University, Kanazawa, Ishikawa 920, Japan

‡ Department of Physics, Japan Atomic Energy Research Institute, Tokai, Ibaraki 319-11, Japan

Received 28 October 1991

Abstract. On the basis of the density-functional theory with the use of the hypernetted-chain approximation, a set of integral equations for the ion–ion and electron–ion radial distribution functions (RDFs) have been derived for a liquid metal as a nucleus–electron mixture; its liquid and electronic structures can be determined from the atomic number Z_A. This formulation is applied to liquid metallic sodium at temperature 100 °C; these integral equations are solved in a self-consistent manner to obtain the ion–ion and electron–ion RDFs, the electron-density distribution of a pseudoatom $\rho(r)$, and the effective interatomic potential $v^{\text{eff}}(r)$ at the same time. The ion–ion structure factor of Na at 100 °C, thus calculated, shows an excellent agreement with the experiment as well as the ion–ion RDF; the effective interatomic potential $v^{\text{eff}}(r)$ giving this ion–ion RDF indicates a quite similar behaviour to that extracted from the measured structure factor by Reatto *et al*, especially near the repulsive-core region. However, the electron–ion RDF and the pseudoatom-electron density $\rho(r)$, obtained recently from the difference between structure factors from x-ray and neutron experiments, show large deviations from the calculated ones; this means that to extract these quantities the experiment should be performed in a more precise manner. For comparison, an effective interatomic potential is constructed by the use of the Ashcroft pseudopotential with a core radius 0.905 Å, which yields almost the same electron–ion RDF and the same screening charge $\rho(r)$ except near the core region in addition to the ion–ion RDF as obtained by the full self-consistent method; the Ashcroft pseudopotential is shown to be appropriate in treating liquid Na in contrast with liquid Li, where it is totally invalid.

1. Introduction

When studying the structure of a simple liquid metal, it is usually treated as a quasi-one-component liquid interacting via an effective interionic interaction determined by a pseudopotential between electron and ion. The pseudopotential method consists of the following three steps: the construction of a pseudopotential, the evaluation of an effective interatomic potential from the pseudopotential, and the determination of a liquid structure from this effective potential using a liquid theory. In the second step, the linear-response theory (the second-order perturbation) is used to calculate the electron screening around an ion; this requires the electron–ion interaction to be weak in the construction of effective interaction. In real liquid metals, the electron–ion correlation is not always so weak. Liquid metallic sodium is known as a typical system with a weak electron–ion interaction. However, it was shown by Dagens,

0953-8984/92/143679+16$04.50

Rasolt and Taylor (DRT) [1] that the non-linear effect in the screening is important even for liquid Na in the evaluation of an effective interatomic potential and that the pseudopotential should be built up so as to produce correctly an electron distribution of a pseudoatom in the form of the usual linear-response expression.

On the other hand, a set of integral equations for radial distribution functions (RDFs) among ions and electrons has been derived on the basis of the density-functional (DF) theory in the quantal hypernetted-chain (QHNC) approximation [2]; the bare ion–electron interaction $\tilde{v}_{eI}(r)$ and the ionic charge Z_I are to be determined self-consistently by viewing a liquid metal as a nucleus–electron mixture [3] in this formulation. This approach is shown to give a non-linear pseudopotential in the same meaning as the DRT treatment, and has already been applied to liquid metallic lithium [4] obtaining the ion–ion structure factors in an excellent agreement with the experiment. Also, it is well known that a usual local-pseudopotential description is not appropriate to liquid lithium due to the absence of p-electron core in contrast to liquid sodium. In fact, the interatomic potential calculated from Ashcroft's model potential is quite different from that by this QHNC formulation, and Ashcroft's model potential cannot give the correct structure for liquid metallic lithium.

Contrary to the fact that a simple description based on a local pseudopotential may be possible for liquid sodium, it is more difficult to apply the QHNC integral equations to this system than to liquid Li, since the inner-core electronic structure is more complicated than that of lithium. Now, we apply the QHNC formulation to liquid metallic sodium. In contrast to a lithium ion with two core electrons, a sodium ion has ten core electrons in liquid metallic state. Therefore, we need some modifications to the numerical procedure to get a fine core–electron structure together with a liquid structure.

Recently, Takeda *et al* [5] have extracted the electron–ion RDF of liquid metallic sodium in addition to several polyvalent metals [6], from the analysis of the difference between structure factors measured by the neutron and x-ray scattering. However, so far there has been no calculation of the electron–ion RDF, especially in the core region, to be compared with these experiments. It is an important experiment to determine the electron–ion RDF, since it involves information on the electron screening of a pseudoatom, which is strongly related to an electron–ion pseudopotential. If the electron–ion RDF can be experimentally obtained with a sufficient precision, we can have a criterion to judge which pseudopotential yields more correctly an effective interionic potential. With this respect, the QHNC formulation can afford to give the electron–ion RDF including the core-region, as well as the ion–ion RDF; the non-linear pseudopotential and effective interionic potential are also determined to be self-consistent with these RDFs using the atomic number as the only input.

The layout of this paper is as follows. We begin in section 2 with a summary of the QHNC integral equations for a liquid metal as a nucleus–electron mixture. In section 3 we describe some approximations applied to liquid metallic sodium and the procedure for the numerical calculation. The results of the QHNC formulation are compared with experiments and other calculations in section 4. The last section is devoted to discussion on the results.

2. Summary of formulation

As a first approach, a liquid metal is regarded as a mixture consisting of ions, with charge Z_I and density n_0^I, and electrons with density n_0^e; the ions form a classical

fluid and the electrons behave as a quantum fluid. Of particular importance in the evaluation of pair correlations in an ion–electron mixture is the fact that the ion–ion and electron–ion RDFs are shown to be equal to the inhomogeneous ion and electron distributions around a fixed ion in a liquid metal, when an ion is a classical particle in the sense that its coordinate and momentum are commutable with each other. From this fact, the DF theory can give exact expressions for the ion–ion and electron–ion RDFs $g_{iI}(r)$ $(i = \mathrm{I}, \mathrm{e})$ using the density-distribution functions $n_i^0(r|v_{ij}^{\mathrm{eff}})$ of non-interacting systems under the effective external potentials $v_{ij}^{\mathrm{eff}}(r)$ in the forms [2]

$$g_{\mathrm{II}}(r) = n_{\mathrm{I}}^0(r|v_{\mathrm{II}}^{\mathrm{eff}})/n_0^{\mathrm{I}} \equiv \exp(-\beta v_{\mathrm{II}}^{\mathrm{eff}}(r)) \tag{1}$$

$$g_{\mathrm{eI}}(r) = n_{\mathrm{e}}^0(r|v_{\mathrm{eI}}^{\mathrm{eff}})/n_0^{\mathrm{e}}. \tag{2}$$

Here, $n_{\mathrm{e}}^0(r|U)$ is obtained by solving the Schrödinger equation for an electron under the external potential $v_{\mathrm{eI}}^{\mathrm{eff}}(r)$, and the effective interaction $v_{\mathrm{iI}}^{\mathrm{eff}}(r)$ is represented by the bare interaction $v_{\mathrm{iI}}(r)$, the direct correlation functions (DCF) $C_{ij}(r)$ and the bridge function $B_{\mathrm{iI}}(r)$ as follows:

$$v_{\mathrm{iI}}^{\mathrm{eff}}(r) = v_{\mathrm{iI}}(r) - \Gamma_{\mathrm{iI}}(r)/\beta - B_{\mathrm{iI}}(r)/\beta \tag{3}$$

with

$$\Gamma_{\mathrm{iI}}(r) \equiv \sum_{l} \int C_{\mathrm{i}l}(|\boldsymbol{r} - \boldsymbol{r}'|) n_0^l [g_{l\mathrm{I}}(r') - 1] \, \mathrm{d}\boldsymbol{r}'. \tag{4}$$

From the definition of the DCFs for the ion–electron mixture, the partial structure factors $S_{ij}(Q)$ are shown to be expressed in terms of DCFs $C_{ij}(Q)$ [2] as

$$S_{\mathrm{II}}(Q) = (1 - n_0^{\mathrm{e}} C_{\mathrm{ee}}(Q)\chi_Q^0)/D(Q) \tag{5}$$

$$S_{\mathrm{eI}}(Q) = \sqrt{n_0^{\mathrm{I}} n_0^{\mathrm{e}}} C_{\mathrm{eI}}(Q)\chi_Q^0/D(Q) = \rho(Q) S_{\mathrm{II}}(Q)/\sqrt{Z_{\mathrm{I}}} \tag{6}$$

with

$$D(Q) \equiv [1 - n_0^{\mathrm{I}} C_{\mathrm{II}}(Q)][1 - n_0^{\mathrm{e}} C_{\mathrm{ee}}(Q)\chi_Q^0] - n_0^{\mathrm{e}} n_0^{\mathrm{I}} C_{\mathrm{eI}}^2(Q)\chi_Q^0 \tag{7}$$

$$\rho(Q) \equiv n_0^{\mathrm{e}} C_{\mathrm{eI}}(Q)\chi_Q^0/[1 - n_0^{\mathrm{e}} C_{\mathrm{ee}}(Q)\chi_Q^0]. \tag{8}$$

Here, χ_Q^0 indicates the density–density response function of a non-interacting electron gas. At this stage, note that equation (6) can be rewritten by the inverse Fourier transform as

$$n_0^{\mathrm{e}} g_{\mathrm{eI}}(r) = \rho(r) + n_0^{\mathrm{I}} \int \rho(|\boldsymbol{r} - \boldsymbol{r}'|) \, g_{\mathrm{II}}(r') \, \mathrm{d}\boldsymbol{r}' \tag{9}$$

which states that the electron–ion RDF is expressed by a superposition of neutral pseudoatoms [7] with an electron distribution $\rho(r)$. In the pseudopotential theory,

a pseudoatom-charge distribution $\rho(Q)$ is expressed by a pseudopotential $w_b(Q)$ in the form:

$$\rho(Q) = -n_0^e \beta w_b(Q)\chi_Q^0/[1 + n_0^e \beta v_{ee}(Q)(1 - G^{jell}(Q))\chi_Q^0] = -n_0^e \beta w_b(Q)\chi_Q^{jell} \tag{10}$$

which is derived by the use of the linear-response formula with the density response function χ_Q^{jell} of an electron gas. Therefore, the expression (10) is valid only for a liquid metal with a weak electron–ion interaction, while (8) is an exact expression for a pseudoatom-charge distribution, provided that a liquid metal can be taken as an ion–electron mixture. At this point, it should be noted that a linear-response expression (10) can be obtained from (8) by the following replacement: $C_{eI}(Q) \simeq -\beta w_b(Q)$ and

$$C_{ee}(Q) \equiv -\beta v_{ee}(Q)(1 - G(Q)) \simeq -\beta v_{ee}(Q)(1 - G^{jell}(Q)) \equiv C_{ee}^{jell}(Q) \tag{11}$$

which means that the local-field correction (LFC) in the ion–electron mixture is approximated by that of the jellium model, $G^{jell}(Q)$. Since $w_b^{nl}(Q) \equiv -C_{eI}(Q)/\beta$ gives an exact expression for $\rho(Q)$ in (8), we can think of $-C_{eI}(Q)/\beta$ as a non-linear pseudopotential in the sense that it can generate a non-linear screening $\rho(r)$ in the form of the linear-response expression. Furthermore, the Ornstein–Zernike (OZ) relations for an ion–electron mixture are described as

$$g_{II}(r) - 1 = C_{II}(r) + \Gamma_{II}(r) \tag{12}$$

$$g_{eI}(r) - 1 = \hat{B}C_{eI}(r) + \hat{B}\Gamma_{eI}(r) \tag{13}$$

which are obtained by the combined use of (5) and (6). Here, $\hat{B}$ denotes an operator defined by

$$\mathcal{F}_Q[\hat{B}^\alpha f(r)] \equiv (\chi_Q^0)^\alpha \mathcal{F}_Q[f(r)] = (\chi_Q^0)^\alpha \int e^{iQ\cdot r} f(r)\,dr \tag{14}$$

for an arbitrary real number α.

In reality, we can regard the ion–electron mixture as a one-component fluid interacting via an effective potential $v^{eff}(r)$, which is defined by the relation:

$$v_{II}^{eff}(r) = v_{II}(r) - \Gamma_{II}(r)/\beta - B_{II}(r)/\beta \equiv v^{eff}(r) - \gamma(r)/\beta - B_{II}(r)/\beta \tag{15}$$

with the DCF $C(r)$ of one-component system and

$$\gamma(r) \equiv n_0^I \int C(|r - r'|)[g_{II}(r') - 1]\,dr'. \tag{16}$$

This effective potential is explicitly written from (15) as

$$\beta v^{eff}(Q) = \beta v_{II}(Q) - C_{eI}^2(Q)\frac{n_0^e \chi_Q^0}{1 - n_0^e C_{ee}(Q)\chi_Q^0} \tag{17}$$

owing to the relation: $\gamma(r) = \Gamma_{II}(r) + \kappa(r)$, with

$$\mathcal{F}_Q[\kappa(r)] \equiv C_{eI}^2(Q)\frac{n_0^e\chi_Q^0}{1 - n_0^e\chi_Q^0 C_{ee}^{jell}(Q)}. \tag{18}$$

Moreover, it is shown that a liquid metal treated more fundamentally as a nucleus–electron mixture can be regarded as an ion–electron mixture with explicit expressions for a bare electron–ion interaction [3]

$$\tilde{v}_{eI}(r) = -\frac{Z_A e^2}{r} + \int v_{ee}(|\mathbf{r} - \mathbf{r}'|)n_e^b(r')\,d\mathbf{r}' + \mu_{XC}(n_e^b(r) + n_0^e) - \mu_{XC}(n_0^e) \tag{19}$$

and the ionic charge Z_I given by

$$Z_I = Z_A - \int n_e^b(r)\,d\mathbf{r} \tag{20}$$

in terms of the exchange-correlation potential μ_{XC} and bound-electron distribution $n_e^b(r) \equiv n_e^{0b}(r|v_{eI}^{eff})$; $\tilde{v}_{eI}(r)$ and Z_I are to be determined in a consistent way to a liquid structure. This definition of Z_I is valid only for a simple metal, where there is no overlapping of bound-electron distributions $n_e^b(r)$ among ions and no resonance state exists. In the nucleus–electron model, the free-electron part of the density distribution $n_e^0(r|v_{eI}^{eff}) = n_e^{0b}(r|v_{eI}^{eff}) + n_e^{0f}(r|v_{eI}^{eff})$ is taken to be the electron–ion RDF, while the bound-electron part is thought to be composed of an ion in a liquid metal.

3. Application to liquid metallic sodium

A set of integral equations for the RDFs $g_{iI}(r)$ is rewritten in the form of integral equations for the DCFs $C_{iI}(r)$ with the help of the OZ relations (12) and (13):

$$C_{II}(r) = \exp[-\beta v_{II}(r) + \Gamma_{II}(r) + B_{II}(r)] - 1 - \Gamma_{II}(r) \tag{21}$$

$$\hat{B}C_{eI}(r) = n_e^{0f}(r|\tilde{v}_{eI} - \Gamma_{eI}/\beta - B_{eI}/\beta)/n_0^e - 1 - \hat{B}\Gamma_{eI}(r) \tag{22}$$

since $\Gamma_{iI}(Q)$ can be described in terms of the DCFs $C_{ij}(Q)$

$$\Gamma_{iI}(Q) = [C_{iI}(Q) - \delta_{iI}n_0^e\chi_Q^0(C_{II}(Q)C_{ee}(Q) - C_{eI}^2(Q))]/D(Q) - C_{iI}(Q). \tag{23}$$

For equations, (21) and (22), to be a closed set of integral equations determining the DCFs, we must introduce the following four approximations:

(i) the LFC $G(Q)$ is taken to be that of jellium model, $G^{jell}(Q)$, in treating the electron-electron DCF $C_{ee}(Q)$, and

(ii) the ion–ion bridge function $B_{II}(r)$ is approximated by $B_{PY}(r;\eta)$ from the Percus–Yevick equation for hard spheres of diameter σ in the same spirit as the modified HNC equation [8];

(iii) the electron–ion bridge function $B_{eI}(r)$ is neglected; and finally the last approximation:

(iv) $v_{II}(r) \simeq Z_I^2 e^2/r$. Here, η is the packing fraction defined by $\eta \equiv \pi n_0^I \sigma^3/6$, and this parameter η in $B_{PY}(r;\eta)$ is determined by the Lado criterion [9]:

$$\int [g_{II}(r) - g_{PY}(r)] \frac{\partial B_{PY}(r;\eta)}{\partial \eta} \mathrm{d}r = 0 \tag{24}$$

with $g_{PY}(r)$ being the RDF for Percus–Yevick equation. In this calculation, we choose the LFC $G^{jell}(Q)$ to be that of Geldart and Vosko [10]:

$$G^{jell}(Q) = q^2/(2q^2 + 4g) \tag{25}$$

with $q = Q/Q_F, g = 1/(1 + 0.0155\alpha\pi r_s), \alpha = (4/9\pi)^{1/3}$ and $r_s = (3/4\pi n_0^I)^{1/3}$ in units of the Bohr radius a_B and the Fermi wavevector Q_F. On the other hand, the exchange–correlation potential μ_{XC} involved in the bare electron–ion interaction $\tilde{v}_{eI}(r)$ of (19) is taken to be that proposed by Gunnarsson and Lundqvist [11]:

$$\mu_{XC}(r_s) = -\frac{2}{\pi\alpha r_s}[1 + 0.0545 r_s \ln(1 + 11.4/r_s)] \text{ Ryd.} \tag{26}$$

Thus, (21) and (22) with these approximations constitute a closed set of integral equations for $C_{II}(r)$ and $C_{eI}(r)$ to be solved self-consistently. Hereafter, we refer to this set of integral equations as the QHNC equations.

The atomic number Z_A and the ionic valency Z_I of sodium in a liquid state are 11 and 1, respectively: two electrons in the 1s state, two electrons in the 2s state, and six electrons in the 2p state forming an ion. A liquid state of Na as an ion–electron mixture can be specified by two parameters: the plasma parameter $\Gamma \equiv \beta e^2/a$ and $r_s \equiv a/a_B$, where the average spherical radius a is defined by $(3/4\pi n_0)^{1/3}$ with $n_0 \equiv n_0^I = n_0^e$. When the QHNC integral equations, (21) and (22), are solved by an iterative procedure, it is important to find initial data as near as possible to the real solution. Liquid metallic sodium near melting point (97.9 °C) has a large plasma parameter $\Gamma \sim 200$ and a large $r_s \sim 4$; therefore, we cannot get a convergent solution for this system because of these large state parameters, if the initial data are not sufficiently close to the real solution.

As the first step to obtain good initial data, we set up an approximate integral equation from (21) and (22). For this purpose, we introduce an approximation to $g_{II}(r)$ by the step function $\theta(r - R)$:

$$g_{II}(r) \approx \theta(r - R) = \begin{cases} 0 & \text{for } r < R \\ 1 & \text{for } r \geqslant R \end{cases} \tag{27}$$

with R being the Wigner–Seitz radius in addition to the approximation $C_{eI}(r) \simeq Z_I e^2/r$. These two approximations reduce the effective electron–ion interaction (3) to the form

$$v_{eI}^{eff}(r) = \tilde{v}_{eI}(r) + f(r) - \bar{\Gamma}_{eI}(r)/\beta \tag{28}$$

and alter (22) in the form

$$\hat{B}\left(C_{eI}(r) - n_0^e \int \beta \frac{e^2}{|r - r'|}[\theta(r' - R) - 1]\,\mathrm{d}r'\right) = n_e^{0f}(r|\tilde{v}_{eI} + f - \bar{\Gamma}_{eI}/\beta)/n_0^e - 1 - \hat{B}\bar{\Gamma}_{eI}(r) \tag{29}$$

with the definition of new functions

$$\bar{\Gamma}_{eI}(r) \equiv \int C_{ee}^{jell}(|r - r'|) n_0^e [g_{eI}(r) - 1] \, dr' \tag{30}$$

$$f(r) \equiv \begin{cases} Z_I e^2 [3 - (r/R)^2]/2R & \text{for } r < R \\ Z_I e^2 / r & \text{for } r \geqslant R \end{cases}. \tag{31}$$

By the combined use of the Fourier transform of (29) and (30), we obtain the following relation:

$$\bar{\Gamma}_{eI}(Q) = \frac{n_0^e \chi_Q^0 C_{ee}^{jell}(Q)}{1 - n_0^e \chi_Q^0 C_{ee}^{jell}(Q)} \left(C_{eI}(Q) - \beta \frac{4\pi e^2}{Q^2} n_0^e \mathcal{F}_Q [\theta(r - R) - 1] \right). \tag{32}$$

Thus, equation (29) with (32) becomes an integral equation for $\bar{C}_{eI}(r)$ defined by

$$\bar{C}_{eI}(r) \equiv C_{eI}(r) - n_0^e \int \beta \frac{e^2}{|r - r'|} [\theta(r' - R) - 1] \, dr' \tag{33}$$

since $\bar{\Gamma}_{eI}(r)$ is expressible in terms of $\bar{C}_{eI}(r)$ by means of (32). In other words, (29) is an integral equation for the electron–ion DCF $C_{eI}(r)$ in the jellium–vacancy model, since the effective electron–nucleus potential (28) is equal to a potential for an electron caused by a nucleus fixed at the centre of spherical vacancy with a radius R in the jellium background.

In order to solve the integral equation (29) for $\bar{C}_{eI}(r)$, it is necessary to set up the initial guesses for $\bar{\Gamma}_{eI}(Q)$ and for the effective electron–nucleus potential $v_{eI}^{eff}(r)$. The first guess for $\bar{\Gamma}_{eI}(Q)$ is obtained from (32) by the use of the approximation that the electron–ion DCF $C_{eI}(Q)$ is replaced by the Ashcroft model potential $w_b^{AC}(Q)$:

$$C_{eI}(Q) \simeq -\beta w_b^{AC}(Q) = \beta \frac{4\pi e^2}{Q^2} \cos(R_c Q) \tag{34}$$

with a core radius $R_c = 0.905$ Å for liquid sodium, and the initial electron–nucleus potential $\tilde{v}_{eI}(r)$ is approximated by the atomic potential proposed by Green *et al* [12]

$$\tilde{v}_{eI}(r) \simeq -\frac{e^2}{r} [(Z_A - 1)\Omega(r) + 1] \tag{35}$$

$$\Omega(r) \equiv [H(e^{r/d} - 1) + 1]^{-1} \tag{36}$$

with $H = 0.72 Z_A^{1/3}$ and $d = 0.57 a_B$; these two approximations afford, also, to give the initial potential (28) generating the electron–ion RDF in (29). In this way, the integral equation (29) can be solved iteratively from these initial data to arrive at the initial $C_{eI}(Q)$, which enables us to evaluate the effective ion–ion interaction $v^{eff}(r)$ from (17).

In the second step, a new ion–ion RDF is calculated from (21), which is rewritten in the form of the integral equation for the DCF $C(r)$ of a quasi-one-component fluid:

$$C(r) \equiv C_{II}(r) - \kappa(r) = \exp[-\beta v^{eff}(r) + \gamma(r) + B_{PY}(r; \eta)] - 1 - \gamma(r) \tag{37}$$

with an effective interatomic potential $v^{\rm eff}(r)$ determined from (17) using a non-linear pseudopotential $w_{\rm b}^{\rm nl}(Q) \equiv -C_{\rm eI}(Q)/\beta$. Here, note that this equation is the modified HNC equation [8] for a one-component fluid; the output $C_{\rm eI}(Q)$ at the first step based on the jellium–vacancy model can be used to produce $v^{\rm eff}(r)$ for the first input potential to (37). By solving this equation, we obtain a new $g_{\rm II}(r)$ and $C_{\rm II}(r)$ to be used as input for the next step.

In the third step, equation (22) is regarded as constituting an integral equation for $C_{\rm eI}(r)$ by thinking of $g_{\rm II}(r)$ and $C_{\rm II}(r)$ as known quantities obtained from the second step; this equation yields new $C_{\rm eI}(r)$ and $\tilde{v}_{\rm eI}(r)$ to be used for the second step in the iterative process. After several repetitions of the second and third steps, we can obtain sufficiently convergent $g_{\rm II}(r)$ and $g_{\rm eI}(r)$, that is $C_{\rm II}(r)$, $C_{\rm eI}(r)$ and $\tilde{v}_{\rm eI}(r)$, which can be used as initial input to the QHNC integral equations, (21) and (22), determining $g_{\rm II}(r)$ and $g_{\rm eI}(r)$ at the same time as the final step. It is found in this procedure that we must repeat the second and third steps so many times that we get such initial input data as to lead to convergent $g_{\rm II}(r)$ and $g_{\rm eI}(r)$ simultaneously from (21) and (22). The whole process to solve a set of integral equations, (21) and (22) is summarized as is shown in the following flow chart.

The first step: $C_{\rm eI}(r), \tilde{v}_{\rm eI}(r) \Longleftarrow$ jellium–vacancy model: (29)

$$\Downarrow$$

$$(17) \quad \Longleftarrow C_{\rm eI}(r), \tilde{v}_{\rm eI}(r) \quad \Longleftarrow \text{the third step: (22)}$$

$$\Downarrow \qquad\qquad\qquad\qquad \Uparrow$$

$$v^{\rm eff}(r) \quad \Longrightarrow \text{the second step: (37)} \quad \Longrightarrow g_{\rm II}(r), \tilde{v}_{\rm eI}(r)$$

$$\Downarrow$$

initial guesses: $C_{\rm II}(r), C_{\rm eI}(r), \tilde{v}_{\rm eI}(r) \Longrightarrow$ (21), (22).

When we solve (37) at the last time in this loop, the parameter η in the bridge function $B_{\rm PY}(r;\eta)$ is determined by the Lado criterion [9].

In the numerical calculation, the fast Fourier transform with respect to $x = r/a$ is adopted to solve integral equations for the RDFs on a 1024 point mesh with an equally-spaced interval $\Delta x = 0.025$. In the evaluation of $n_{\rm e}^0(r|v_{\rm eI}^{\rm eff})$, the Schrödinger equation is solved on a finer mesh modified from the Herman–Skillman code [13] to represent a fast oscillation of the wavefunction near the origin. Bound states are calculated on the mesh consisting of 11 blocks: the first block containing 80 points with the interval δ_7, the eighth block of 160 points with δ_0 and another block of 40 points, using the interval doubled in each successive block according as $\delta_l \equiv \Delta x/2^l$ $(l = 7, 6, \ldots, -4)$, respectively. On the other hand, the Schrödinger equation for a scattering state is integrated on the mesh composed of four blocks: the first block involving 80 points with δ_3, 40 points with δ_2, 40 points with δ_1 and 480 points with δ_0, respectively.

4. Results of calculation

In this section, the QHNC formulation [2, 3] is used to calculate the structure of liquid metallic sodium at 100 °C near the melting point with the use of the procedure described in the previous section. Liquid sodium at this temperature has the number density $n_0 = 2.43 \times 10^{-2}$ Å^{-3} [14], which yields two state parameters: $\Gamma = 209.1$ and $r_{\rm s} = 4.046$. The QHNC integral equations are solved in a self-consistent manner under this condition; the packing fraction η in the bridge function $B_{\rm PY}(r;\eta)$ is found to be $\eta = 0.468$ from the Lado criterion (24). It is to be noted at this point

that if the electron–ion DCF $C_{eI}(r)$ is given beforehand, the QHNC formulation has only one unknown function $C_{II}(r)$, which should be determined by (21), that is by (37); after solving this equation, the electron–ion RDF and the screening charge of a pseudoatom can be evaluated by the use of (6) and (8), respectively. For comparison to the full QHNC results, we carry out this calculation for liquid metallic sodium at same temperature adopting Ashcroft's model potential $w_b^{AC}(r)$ to approximate $C_{eI}(r)$:

$$C_{eI}(r) = -\beta w_b^{AC}(r) = \begin{cases} 0 & \text{for } r < R_c \\ \beta Z_I e^2/r & \text{for } r \geqslant R_c \end{cases} \tag{38}$$

with a core radius $R_c = 0.905$ Å [15]. The packing fraction η in the modified HNC equation becomes $\eta = 0.471$ for the interatomic potential from this pseudopotential; the results obtained by the use of the pseudopotential are also given below.

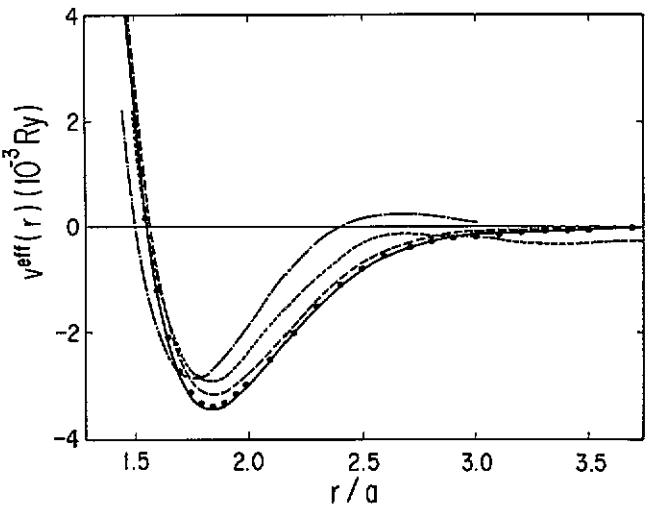

Figure 1. Effective interatomic potentials $v^{eff}(r)$ calculated for liquid sodium at 100 °C with state parameters $\Gamma = 209.1$ and $r_s = 4.046$: Full curve, the full self-consistent QHNC method; broken curve, the use of the jellium–vacancy model; solid circles, the pseudopotential method using Ashcroft's model potential with $R_c = 0.905$Å. The dotted curve denotes the potential $v^{eff}(r)$ extracted from the measured structure factor by Reatto *et al* [17], while the chained curve indicates $v^{eff}(r)$ of Perrot and March [14].

In the first place, figure 1 exhibits the effective interatomic potential $v^{eff}(r)$ calculated by the QHNC method (the full curve), which is consistent with the electron–ion and ion–ion RDFs, in comparison with other results. The QHNC potential shows a quite similar behaviour as that (the dotted curve) extracted from the measured structure factor [16] by Reatto *et al* [17], especially near the repulsive core region; positions of potential minimum coincide with each other. On the other hand, the broken curve is the interatomic potential calculated at the first step by the use of jellium–vacancy model, which is used to obtain initial data to solve the QHNC integral equations; this treatment is shown to yield even at this stage a well approximated potential to the full consistent QHNC potential denoted by the full curve. It should be remarked that the procedure to evaluate this potential is essentially the same as the DRT method [1] and that used by Perrot *et al* [14, 18–20] in the sense that a pseudopotential in the linear-response expression is built up so as to generate a non-linear screening charge of a pseudoatom determined by the DF theory with the help of the jellium–vacancy model. It is also interesting that the empty-core model potential proposed by Ashcroft produces an interatomic potential which is almost

coincident with the QHNC one as denoted by the full circles in figure 1, if the core radius R_c is taken to be 0.905 Å [15]; this core radius generates almost the same $\rho(Q)$ as the QHNC electron screening of a pseudoatom as is shown in figure 5. The chain curve in figure 1 is the result calculated by Perrot and March [14] based on the jellium–vacancy model; their potential, however, shows a disagreement with the QHNC one, and then they [20] propose the scaled potential $v^{\text{eff}}(\mu r)$ using a constant $\mu = 0.9564$ to get a better fit to that extracted by Reatto *et al.* The interatomic potential calculated by Rasolt and Taylor [1], though at a slightly different r_s, is much shallow at the minimum with a value of -2×10^{-3} Ryd, but its minimum position coincides with the QHNC potential.

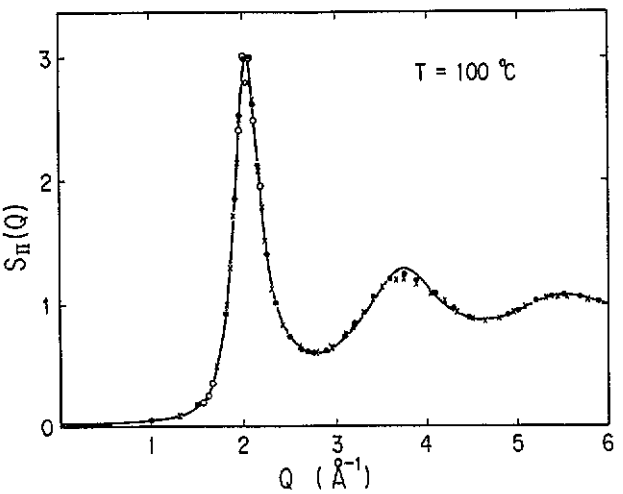

Figure 2. Ion–ion structure factor $S_{II}(Q)$ for liquid sodium at 100 °C, obtained by the QHNC calculation (full curve), comparing with x-ray experiment results of Greenfield *et al* [16] (crosses) and of Huijben and van der Lugt [21] (full circles). The open circles indicate a small deviation of the result of the pseudopotential method from the QHNC structure factor.

Next, we display in figure 2 the ion–ion structure factor $S_{II}(Q)$ by the full curve, which is obtained from the modified HNC equation with $\eta = 0.468$ for the QHNC interatomic potential shown in figure 1. Our full consistently calculated structure factor shows an excellent agreement with the experimental results of Huijben and van der Lugt [21] denoted by full circles and of Greenfield *et al* [16] plotted by crosses; the first peak of our result is slightly higher than that of Greenfield *et al* and lower than that of Huijben and van der Lugt, and the second peak deviates to the higher side compared with the experiments, however. The same difference of the peak height from the experiment is seen in the structure factor obtained by Perrot and Chabrier [20] using the scaled potential. In addition, the structure factor calculated by the modified HNC equation with $\eta = 0.471$ for a potential from the Ashcroft pseudopotential becomes almost identical with the QHNC result with quite small difference in the first peak as is shown by open circles in figure 2. Also, the structure factor $S_{II}(0)$ at zero wavevector, which is related with the compressibility, is obtained as 0.031 by the QHNC calculation, while the structure factor $S_{II}(0)$ from the Ashcroft potential is 0.029; these values are to be compared with the experimental ones: 0.024 (Greenfield *et al*) and 0.026 (Huijben and van der Lugt).

Figure 3 shows the ion–ion RDFs $g_{II}(r)$ obtained from the inverse Fourier transform of the structure factors of figure 2. The RDF from our self-consistent calculation represented by the full curve is compared with the RDF obtained from the experimental structure factor by Huijben and van der Lugt (full circles) and the Monte Carlo

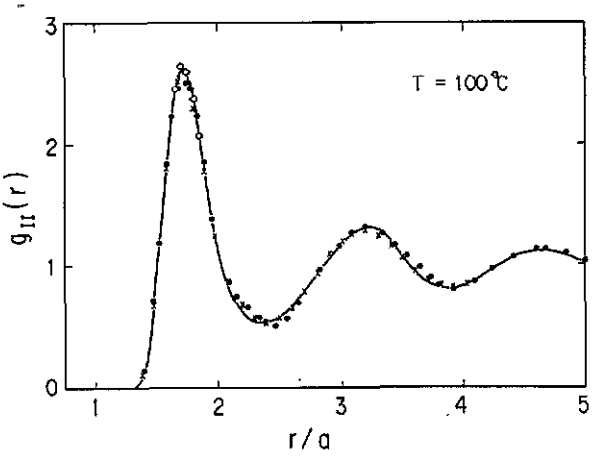

Figure 3. Ion–ion radial distribution functions $g_{II}(r)$ for liquid sodium at 100 °C, calculated by the QHNC method (full curve) and the Monte Carlo method [22] (crosses), compared with the experimental one [21] (full circles). The open circles are plotted to show the small difference between the results of the peudopotential and QHNC methods.

RDF of Murphy and Klein [22] (denoted by the crosses) of which Fourier transform gives the structure factor in good agreement with that measured by Greenfield *et al* [16]. Similarly to $S_{II}(Q)$ in figure 2, the RDF obtained by the modified HNC for a potential based on the Ashcroft potential is almost equal to the QHNC RDF; a small deviation is seen near the first peak as shown by the open circles.

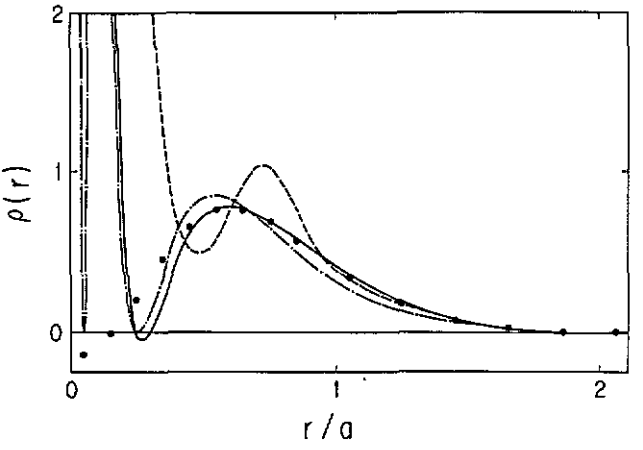

Figure 4. Charge distributions $\rho(r)$ of a neutral pseudoatom in liquid sodium, calculated by the QHNC method (full curve) and the pseudopotential method (full circles), in comparison with the 3s-bound-electron density (chain curve) in a free atom. The broken curve represents the experimental result [23].

In figure 4, we show the valence-electron distribution of a neutral pseudoatom $\rho(r)$, calculated by the QHNC (the full curve) and pseudopotential (full circles) methods, in comparison with the experiment result (the broken curve) and the 3s-bound-electron density (the chain curve) of a free atom. The QHNC $\rho(r)$ plotted by the full curve shows quite similar behaviour to the 3s-bound-electron density of a free atom near its second node and outside the core region. In the QHNC $\rho(r)$, there are two dips near the same positions where the 3s-bound-electron density of a free atom has two nodes, as is displayed in figure 5, where $r^2\rho(r)$ is plotted in units of a^2n_0 for the vertical axis. In figure 4, the density $\rho(r)$ determined by the linear response with the use of the Ashcroft potential is plotted by the full circles, which shows good agreement with the QHNC screening density outside the core region. This agreement

can be seen more clearly in figure 6, which indicates that the QHNC screening density $\rho(Q)$ is almost identical with the pseudopotential $\rho(Q)$ in the Fourier-transformed expression of $\rho(r)$. In other words, we can interpret this fact as meaning that the parameter R_c in the Ashcroft model potential has been chosen so as to produce precisely the non-linear screening. On the other hand, Takeda *et al* [23] extracted the screening charge $\rho(r)$ of a pseudoatom in liquid Na from the difference between structure factors measured by x-ray and neutron diffraction experiments; their result denoted by the broken curve behaves differently from the calculated results.

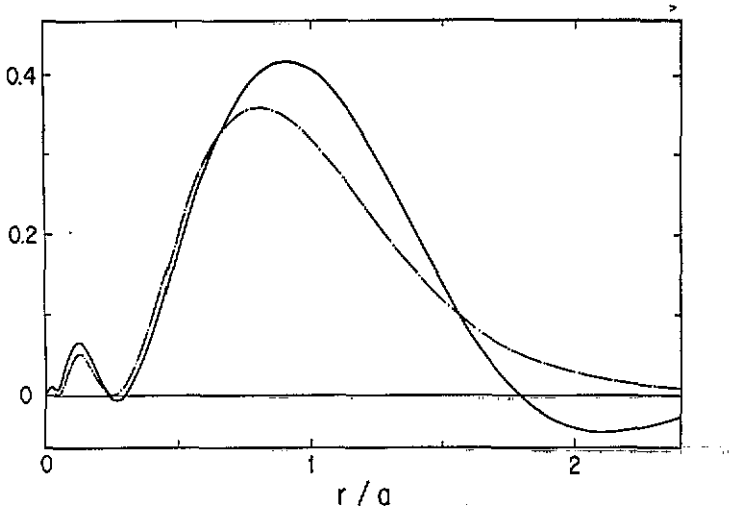

Figure 5. The pseudoatom radial density $r^2\rho(r)$ in liquid sodium, obtained by the QHNC method (full curve) in comparison with the 3s-bound-electron radial density of a free sodium atom.

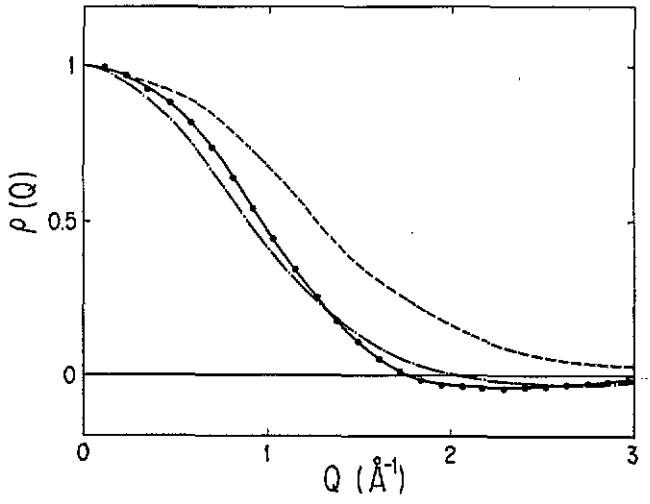

Figure 6. Fourier-transformed charge distributions $\rho(Q)$ of a pseudoatom in liquid sodium: Full curve, the QHNC method; full circles, the pseudopotential method; chain curve, the Fourier transform of the 3s-bound-electron density of a free atom. The experimental result [23] is plotted by the broken curve.

Moreover, figure 7 indicates that the electron–ion RDF $g_{eI}(r)$ from the experiment by Takeda *et al* [5], plotted by the broken curve, shows a quite different behaviour from those calculated by the QHNC (the full curve) and pseudopotential (the full circles) methods, while the RDF $g_{eI}(r)$ based on the Ashcroft potential becomes identical with the QHNC $g_{eI}(r)$ outside of the core-region. In particular, the electron–ion structure factor $S_{eI}(Q)$ obtained by the experiment (full circles) seems to have no common feature to the calculated $S_{eI}(Q)$ in figure 8. The QHNC $g_{eI}(r)$, which is determined as the valence-electron distribution around a fixed nucleus at the origin, has also two dips at $r/a \sim 0.05$ and 0.27, corresponding to the dips of $\rho(r)$ in figure 5. The inner dip is not plotted in this figure due to its large value $g_{eI} \sim 2.4$. These dips can be associated with the existence of the bound electrons in an ion. According to Perrot and March [14], each average of square of the distance of the orbitals of bound electrons, $\sqrt{\langle r^2 \rangle}/a$, is 0.04 for 1s, 0.22 for 2s and 0.23 for 2p state in units of the average ion distance a; the outer and bigger dip in the QHNC $g_{eI}(r)$ comes from the repulsion by Pauli's principle due to eight electrons in the 2s and 2p states, and the inner and smaller dip is ascribed to the core repulsion due to two electrons in the 1s state. On the other hand, the dip in the experimental $g_{eI}(r)$ is near 4.8, however. Therefore, it is appropriate to think that this disagreement is caused by an inaccuracy in the experiment.

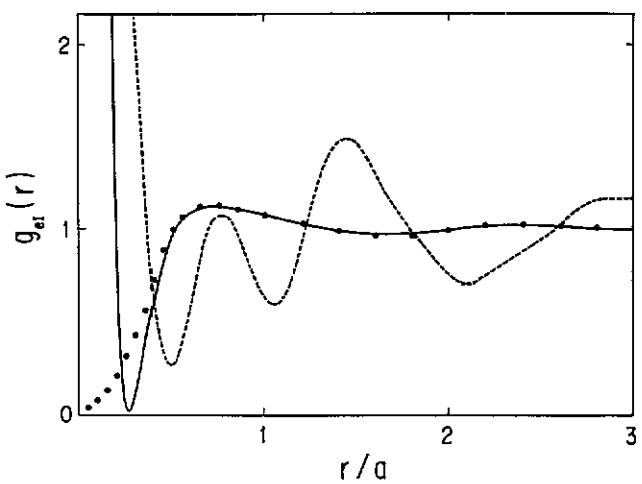

Figure 7. Electron–ion radial distribution functions $g_{eI}(r)$ for liquid sodium: Full curve, the QHNC method; full circles, the pseudopotential method; broken curve, the experimental result [5].

5. Conclusion and discussion

It is shown that the whole electronic and ionic correlations of liquid metallic sodium at temperature 100 °C can be determined by the QHNC formulation on the basis of the nucleus–electron model using atomic number Z_A as only input data. The electronic structure of an ion in a liquid state is also determined in a consistent way to the surrounding ionic and electronic structure; the self-consistent potential $v_{eI}^{eff}(r)$

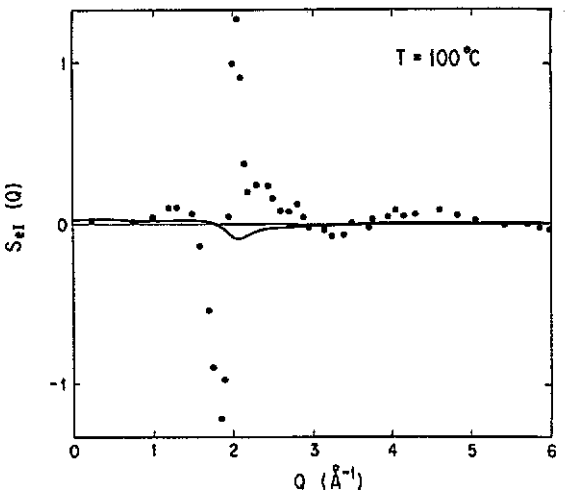

Figure 8. Electron–ion structure factor $S_{eI}(Q)$ of liquid sodium, calculated by the QHNC method (full curve) in comparison with the extracted result from the difference between the neutron and x-ray experiments [5] (full circles).

under the circumstance supports only three bound energy levels (1s,2s,2p), which is consistent with the ionic charge being $Z_I = 1$ due to a delocalized 3s electron.

In this formulation, the RDF $g_{eI}(r)$ gives the screening cloud $\rho(r)$ which contains information of a non-linear pseudopotential $w_b^{nl}(Q) \equiv -C_{eI}(Q)/\beta$, which determines the effective interatomic potential $v^{eff}(r)$ to yield the ion–ion RDF $g_{II}(r)$; thus, all these quantities are obtained simultaneously in a self-consistent manner. The ionic structure, $S_{II}(Q)$ and $g_{II}(r)$, calculated from the QHNC formulation show excellent agreement with the experimental results, as shown in figures 2 and 3. However, the electronic structures represented by $\rho(r)$ and $g_{eI}(r)$ as well as their Fourier transforms, $\rho(Q)$ and $S_{eI}(Q)$, show a great difference between the theoretical and experimental results, as is seen from figures 4 to 8.

In this calculation, the LFC $G(Q)$ and the exchange–correlation potential $\mu_{XC}(r_s)$ are introduced from outside the QHNC formulation. In this connection, it is well known that the LFC $G(Q)$ plays a critical role in the determination of an interatomic potential $v^{eff}(r)$ [15, 24]. However, it should be noted that to date there is no criterion by which to judge beforehand which LFC is better for the evaluation of $v^{eff}(r)$, since the LFC $G(Q)$ involved in the expression for $v^{eff}(r)$ of (17) is the LFC of the ion–electron mixture, which is different from the jellium LFC for which we have some knowledge of the conditions to be fulfilled. To take account of the influence of ions on the LFC, it is necessary to set up another equation for $C_{ee}(r)$, as was done in the calculation of liquid metallic hydrogen [2]. In any case, the steep repulsive part of $v^{eff}(r)$, which essentially determines the ion–ion RDF, may remain unaltered as is calculated in figure 1, where the QHNC potential coincides with that extracted from the experimental structure factor by Reatto *et al* [17] in the repulsive core region. In addition, the scaled potential introduced by Perrot and Chabrier [20] to fit the potential of Reatto *et al* [17] is shown to agree with the QHNC interatomic potential near the repulsive-core region with the same position of potential minimum.

It is interesting that the Ashcroft pseudopotential with a core radius $R_c = 0.905$ Å can yield the Fourier-transformed screening cloud $\rho(Q)$ which coincides

with the QHNC $\rho(Q)$ in figure 6; consequently, there is no essential difference between the effective interatomic potentials and the ion–ion and electron–ion RDFs, whether they are calculated by the QHNC or pseudopotential method. This fact makes a strong contrast with the case of liquid lithium [4], where the Ashcroft model potential does not work well. This indicates that liquid sodium is the typical system of a simple metal, where the pseudopotential theory can be applied successfully if the non-linear screening effect is taken into account properly.

In contrast to the ionic structure, the electronic structure such as $\rho(r)$ and $g_{eI}(r)$ do not show any agreement between theoretical and experimental results, as shown in figures 4–8. In the QHNC formulation, the electronic structure $\rho(r)$ determines the effective interatomic potential, as it is understood from the relation:

$$\beta v^{\text{eff}}(Q) = \beta v_{II}(Q) - \rho(Q) C_{eI}(Q) \tag{39}$$

to give the RDF $g_{II}(r)$, which shows an excellent agreement with the experimental results. Also, the QHNC $g_{eI}(r)$ and $\rho(r)$ have an inner-core structures similar to a 3s bound state of a free atom. As a consequence, these facts can be taken as indications that our result for the electronic structure is calculated correctly. In contrast to the calculation, the correlation in the experimental $g_{eI}(r)$ persists over too long a range to produce a proper atomic interaction by (39) with the use of $\rho(Q)$ determined by the relation (6). Therefore, we are forced to demand that the experiment to extract the RDF $g_{eI}(r)$ should be performed with more precision both for the neutron and x-ray diffraction.

Finally, it should be remembered that the QHNC formulation with four approximations in the present work can only be applied to a simple metal, where the core-overlap is negligible and there is no resonant state; to take account of these contributions, the multi-centre problem to evaluate a core-overlap effect must be solved in a coupled manner with the single-centre problem to determine the RDFs [25].

References

[1] Rasolt M and Taylor R 1975 *Phys. Rev.* B **11** 2717
Dagens L, Rasolt M and Taylor R 1975 *Phys. Rev.* B **11** 2726
[2] Chihara J 1986 *Phys. Rev.* A **33** 2575
[3] Chihara J 1984 *J. Phys. C: Solid State Phys.* **17** 1633
[4] Chihara J 1989 *Phys. Rev.* A **40** 4507
[5] Takeda S, Harada S, Tamaki S and Waseda Y 1989 *J. Phys. Soc. Japan* **58** 3999
[6] Takeda S, Tamaki S and Waseda Y 1985 *J. Phys. Soc. Japan* **54** 2552
Takeda S, Tamaki S, Waseda Y and Harada S 1985 *J. Phys. Soc. Japan* **55** 184
Takeda S, Harada S, Tamaki S and Waseda Y 1985 *J. Phys. Soc. Japan* **55** 3437
[7] Ziman J M 1967 *Proc. Phys. Soc.* **91** 701
[8] Rosenfeld Y and Ashcroft N W 1979 *Phys. Rev.* A **20** 1208
[9] Lado F, Foiles S M and Ashcroft N W 1983 *Phys. Rev.* A **28** 2374
[10] Geldart D J W and Vosko J H 1966 *Can. J. Phys.* **44** 2137
[11] Gunnarsson O and Lundqvist B I 1976 *Phys. Rev.* B **13** 4243
[12] Green A E S, Sellin D L and Zachor A S 1969 *Phys. Rev.* **184** 1
[13] Herman F and Skillman S 1967 *Atomic Structure Calculations* (Englewood Cliffs, NJ: Prentice-Hall)
[14] Perrot F and March N H 1990 *Phys. Rev.* A **41** 4521
[15] Hafner J 1987 *From Hamiltonians to Phase Diagrams* (Berlin: Springer)
[16] Greenfield A J, Wellendorf J and Wiser N 1989 *Phys. Rev.* A **4** 1607
[17] Reatto L, Levesque D and Weis J J 1986 *Phys. Rev.* A **33** 3451

[18] Perrot F 1990 *Phys. Rev.* A **42** 4871
[19] Dharma-wardana M W C and Perrot F 1990 *Phys. Rev. Lett.* **65** 76
[20] Perrot F and Chabrier G 1991 *Phys. Rev.* A **43** 2879
[21] Huijben M J and van der Lugt 1971 *Acta Crystallogr.* A **35** 431
[22] Murphy R D and Klein M L 1973 *Phys. Rev.* A **8** 2640
[23] Takeda S, Tamaki S and Waseda Y 1990 *J. Phys.: Condens. Matter* **2** 6451
[24] Duesbery M S and Taylor R 1969 *Phys. Lett.* **30A** 496
Kumaravadivel R and Evans R 1976 *J. Phys. C: Solid State Phys.* **9** 3877
Jacucci G and Taylor R 1981 *J. Phys. F: Met. Phys.* **11** 789
Bretonnet J L and Regnaut C 1984 *J. Phys. F: Met. Phys.* **14** L59
[25] Chihara J 1991 *J. Phys.: Condens. Matter* **3** 8715